Oil & Gas Science and Technology – Rev. IFP Energies nouvelles **75**, 34 (2020)

https://doi.org/10.2516/ogst/2020028

Available online at:
ogst.ifpenergiesnouvelles.fr

Engine Combustion Network – France
Christine Rousselle and Gilles Bruneaux (Guest editors)

REGULAR ARTICLE OPEN ACCESS

Effect of exhaust gas recirculation composition on soot in ECN spray A conditions

Chetankumar Patel, Camille Hespel*, Tung Lam Nguyen, Fabrice Foucher, and Christine Mounaïm-Rousselle

Université d'Orléans, INSA CVL, PRISME, EA 4229, 45072 Orléans, France

Received: 25 November 2019 / Accepted: 8 April 2020

Abstract. Due to its strong impact on health, particulate matter is increasingly regulated by government emission standards for vehicles. As one of the sources of particulate matter is the soot produced by internal combustion engines, it remains a challenge to improve advanced combustion modes to reduce it. There is still, however, some lack of understanding about the formation and oxidation processes of soot, especially in "realistic" conditions, such as for example at high temperature and pressure conditions with or without the presence of exhaust gases. The objective of this study is to investigate soot formation in the case of *n*-Dodecane spray flames at conventional Diesel engine conditions generated in the New One Shot Engine by using diffused back-illumination extinction with different CO_2 and water vapour contents. It was found that CO_2 addition reduces the soot mass fraction if its volumetric concentration in ambient mixtures is at least 4.5% while 1% of water is sufficient to significantly reduce the soot mass fraction. The impact of the ambient mixture obtained in ECN spray A pre-burn vessels was also investigated to assess the accuracy against soot measurements available in the literature.

1 Introduction

Human exposure to soot is responsible for cancer, cardiovascular diseases and respiratory diseases [1]. Soot is an amorphous carbon substance, generally produced during combustion processes. In the case of conventional Diesel combustion, the formation of soot is due to the reduced amount of air available to burn the fuel completely at high temperature and pressure conditions during fuel spray combustion, especially during the diffusion phase [2]. Soot formation is also affected by the presence of other ambient gases such as CO_2 or H_2O [3, 4]. These gases induce (i) a reduction in interparticle interaction caused by dilution (ii) a change in temperature and heat capacity of the flame caused by thermal effects, and (iii) chemical reactions that either oxidize soot or react with gaseous precursors. As, in modern internal combustion engines, one way to strongly reduce NO_X is the recirculation of exhaust gas, the presence of CO_2 or H_2O in the combustion chamber is now usual and can impact soot formation. Several numerical and experimental studies about their effects on ethylene (both premixed and diffusion flames) [5–8] concluded that they have an effect on soot reduction, due especially to chemical effects.

Measuring the volume fraction of soot requires the use of optical diagnostics with optimised signal processing. In the context of the Engine Combustion Network [9], it is mainly measured by means of two optical techniques: light based extinction techniques usually called Diffused Back-Illumination (DBI) and Laser-Induced Incandescence (LII) [10, 11]. The first method is based on the attenuation of light through the soot cloud due to elastic scattering and to absorption by the soot particles. However, in the case of Spray A conditions, *i.e.* 900 K and 60 bar as ambient thermodynamic initial conditions, the beam steering is so strong that it becomes difficult to distinguish absorption- or scattering-induced attenuation [12]. Therefore, Ghandhi and Heim [13] worked on the quality of the collimated light needed for DBI and its transmission within the region of interest. In their study, the collimated light of an automotive headlamp was passed through a pinhole and was collected by a Fresnel lens before being transferred to an engineered diffuser to direct it towards the region. A high intensity pulsating LED with 100 W peak optical power to be used as source for the soot measurement in high pressure-high temperature spray flames was developed recently [12, 14]. This modified technique is considered as the ECN reference. The data obtained in the Constant volume Preburn Vessel (CPV) were compared with simulation results obtained from different soot models coupled with a large-eddy simulation for *n*-Dodecane combustion [10, 15–17] or a k–ε turbulence model [18, 19]. The simulations were validated with 15% of oxygen and various combustion products. To complete the available database

* Corresponding author: camille.hespel@univ-orleans.fr

and to improve modelling concepts, a parametric study on the effects of EGR composition on soot formation for ECN spray A is needed.

In the present study, the New One Shot Engine (NOSE) was used as experimental set-up since the initial conditions required for ECN-spray A are attainable and the ambient mixture composition can be adjusted as desired [20]. The experiments were conducted for Spray A conditions, *i.e.* 900 K and 22.8 kg/m^3 with an oxygen concentration of 15% but with a variation of Nitrogen (N_2) content with the addition of CO_2 (0–7% vol) and H_2O (0–5% vol). Moreover, to evaluate the robustness of previous results obtained in other vessels (such as constant pressure flow or constant pre-burn), the impact of ambient compositions similar to those in a CPV as in [9], *i.e.* 6.22% CO_2 and 3.62% H_2O, on soot production was also explored.

The next Section 2 discusses the experimental setup and conditions, and is followed by Sections 3–5.

2 Experimental setup and conditions

2.1 Experimental facility

The main specifications of NOSE, a one-shot rapid compression machine, and the Spray A – ECN conditions, *i.e.* 900 K, 22.8 kg/m^3, are summarized in Table 1 and fully described in [21]. The *n*-Dodecane fuel was injected through a BOSCH CR2.16 single hole injector at the injection pressure of 150 MPa in the optical chamber filled with a mixture of ambient gases at a constant O_2 percentage of 15% vol (Tab. 2).

2.2 Ambient gas composition matrix

Table 2 shows the different compositions of ambient gases selected with a constant oxygen concentration (15% vol) and the adjustment of N_2, alone, according to the addition of CO_2 and H_2O. Moreover, to perform tests at a constant ambient gas density inside the chamber the back pressure (P_{back}) and the temperature at the injection timing were adjusted. The theoretical adiabatic temperature of the air/fuel mixture for the global equivalence ratio (0.0313) as a function of the ambient gas composition is also indicated.

2.3 Optical techniques

Two optical measurements were simultaneously used. First, the OH* chemiluminescence imaging technique was set up to obtain the Lift-Off Length (LOL) of the flame by using an intensified CMOS camera (Photron – APX-I2) with a UV lens 60 mm f/3.5 and a BP filter centered at 310 nm with FWHM at 10 nm. The frame rate was kept at 2 kHz. During the steady phase of combustion (1800–3000 µs after SOE), three images were analysed following the post-processing recommended by [22].

Second, the measurement of soot was done by DBI, based on the transmission of an initial light with I_0 as intensity. When this light passes through the sooting flame, a certain amount of the light is absorbed and scattered by the soot and the remainder is transmitted to the receiver, with an intensity of I. Using Beer-Lambert's law, the amount of soot can be deduced with the product of the path length, L and the extinction coefficient, K [23]:

$$\frac{I}{I_0} = e^{-KL}. \quad (1)$$

Figure 1 shows the schematic of the DBI setup around NOSE. The light source was generated by a green LED (CBT-120-GC11-JM200) at $\lambda = 532$ nm. The illuminating rays of the LED were transferred to a Fresnel lens with an effective diameter of 63.5 mm and a focal length of 99 mm through a pinhole to generate parallel light beam. Then these rays were transferred to an engineering diffuser to generate a homogeneous distribution of the light in the region of interest. The images of the transmitted light were captured by a Phantom V16 CMOS camera at the frame rate of 45 kHz. An AF Micro-Nikon 50 mm f/1.8 D lens with two filters, a BP filter centered at 532 nm with 10 nm FWHM and a neutral density filter of 75% were used.

The first challenge when applying the DBI technique is to reduce beam steering by choosing the optimal distance between the different optical elements as presented in Figure 1. As indicated in equation (2), the divergence angle of the diffuser, θ must be larger than the sum of the maximum anticipated beam steering angle, α with the acceptance angle of the collecting optics, ω, as underlined in [23]. If the divergence angle of the diffuser is not large enough, then there is a possibility that some area of the extinction beam might be moved out of the imaged area. However, the diffuser used in our setup has a 15° divergence angle θ and the acceptance angle ω of our optics is 8.36°, this system therefore ensures a beam steering angle, α of 6.64° which is large enough to fulfil the first requirement [9]:

$$\theta \geq \alpha + \omega. \quad (2)$$

The second criterion is the size of the collimated beam.The beam diameter, D should be higher than the sum of the probe volume, S and the tangential of the addition of the beam steering angle and the acceptance angle across the length L, between the probe volume and the CMOS

Table 1. Main specifications of new one shot engine for spray A conditions.

Specifications	Value
Volume of the chamber	~0.24l
Injector tip protrusion	6 mm
Wall temperature	373 K
Fuel	*n*-Dodecane
Injection pressure	150 MPa
Orifice diameter	89.7 µm, $K_s = 1.5$, Cd = 0.96
Ambient temperature	900 K
Ambient density	22.8 kg/m^3
Injection duration	~3.2 ms

Table 2. Test conditions.

Nomenclature	Ambient gas composition (% volume)				P_{back} at injection timing (MPa)	T at real injection timing [K] ±4 K	Adiabatic Flame Temperature ($T_{adiabatic}$) K
	O_2	N_2	CO_2	H_2O			
0% CO_2/0% H_2O	15.00	85.00	x	x	6.0	901	957
2% CO_2	15.00	83.00	2.00	x	5.9	901	957
4.5% CO_2	15.00	80.50	4.50	x	5.8	898	954
7% CO_2	15.00	78.00	7.00	x	5.7	890	946
1% H_2O	15.00	84.00	x	1.00	6.0	901	957
2% H_2O	15.00	83.00	x	2.00	6.0	901	957
3% H_2O	15.00	82.00	x	3.00	6.0	900	956
4% H_2O	15.00	81.00	x	4.00	6.0	898	953
5% H_2O	15.00	80.00	x	5.00	6.0	895	950
6.22% CO_2 + 3.63% H_2O	15.00	75.15	6.22	3.63	5.7	889	945

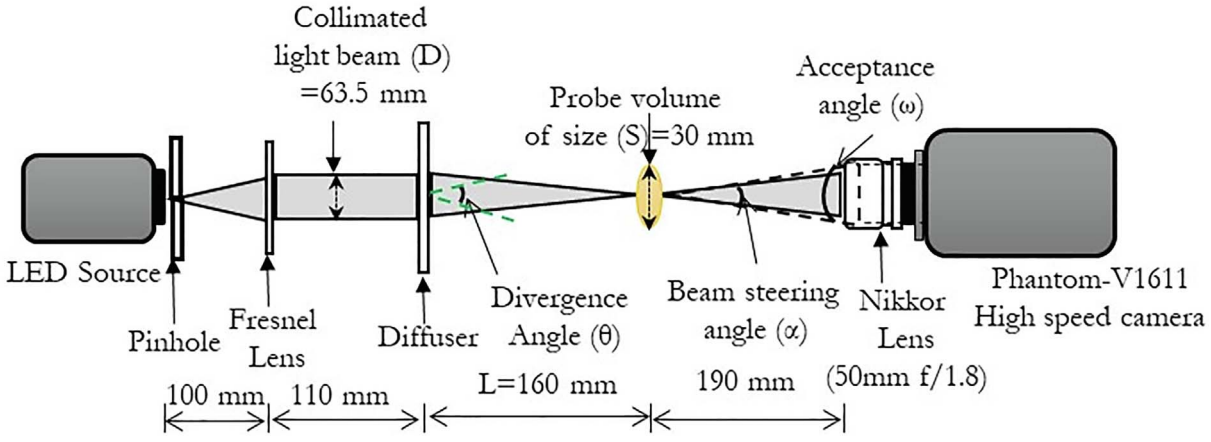

Fig. 1. Detailed optical arrangement at DBI setup.

sensor. If this criterion is not fulfilled, there will be beam steering along the edges of the probe volume,

$$D \geq S + \tan(\alpha + \omega) \cdot L. \tag{3}$$

This is obtained for the present optical setup for a beam steering angle, $\alpha = 2.86°$ [12].

Another issue is the effect of the "negative image lag", due to the incomplete reset of the CMOS sensor during the pixel readout. The residual signal with this negative image lag affects the next image and therefore the estimate of KL. However, this effect can be removed by analysing a third image without LED. In our case a comparison of LED off frame with and without LED pulsing showed that the residual negative signal is negligible. The high speed camera acquired the images with and without LED light, a frame rate of 45 kHz with an exposure time of 3 µs while the LED frequency was kept at 22 500 pulse/sec, as shown in Figure 2. This choice is a good compromise between a good temporal resolution, a high stability of the light-source intensity and very low negative image lag.

2.4 Image processing

Figure 3 describes the different steps followed to post-process the DBI image as recommended in [23] by the ECN. The first image corresponds to when the LED is ON, and consists of the LED signal and the natural luminosity of the soot cloud, I_{LED+NL}. Complete LED-light extinction is never measured. The second image is obtained for the LED off frame and consists purely of the natural luminosity signal, I_{NL}. Images of the background due to the dark noise were previously recorded and due to the CMOS technology, it was considered as to be zero. The third image represents the light intensity without flame and soot, I_0 in the probe volume S. Soot extinction, KL, for one DBI image, j, is obtained thanks to equation (1),

$$KL = -\ln\left(\frac{I_{LED}}{I_0}\right), \tag{4}$$

where $I_{LED} = I_{LED+NL,j} - I_{NL,j-1}$.

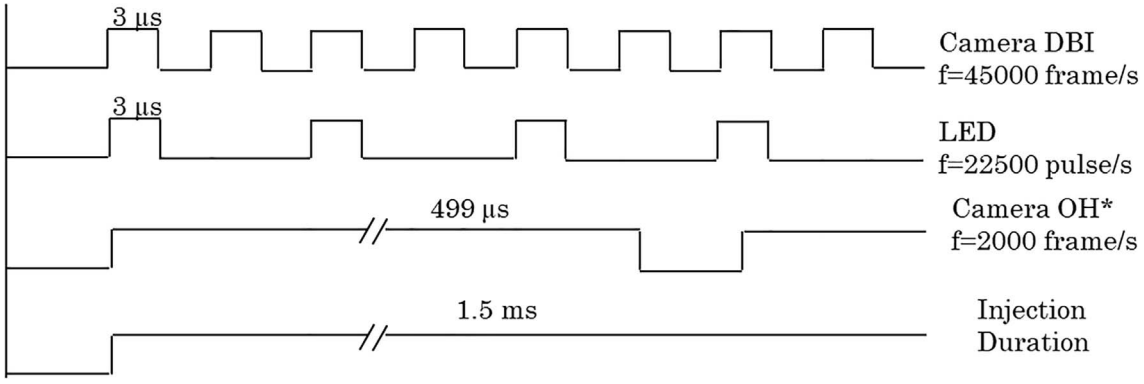

Fig. 2. Signal arrangement for the setup.

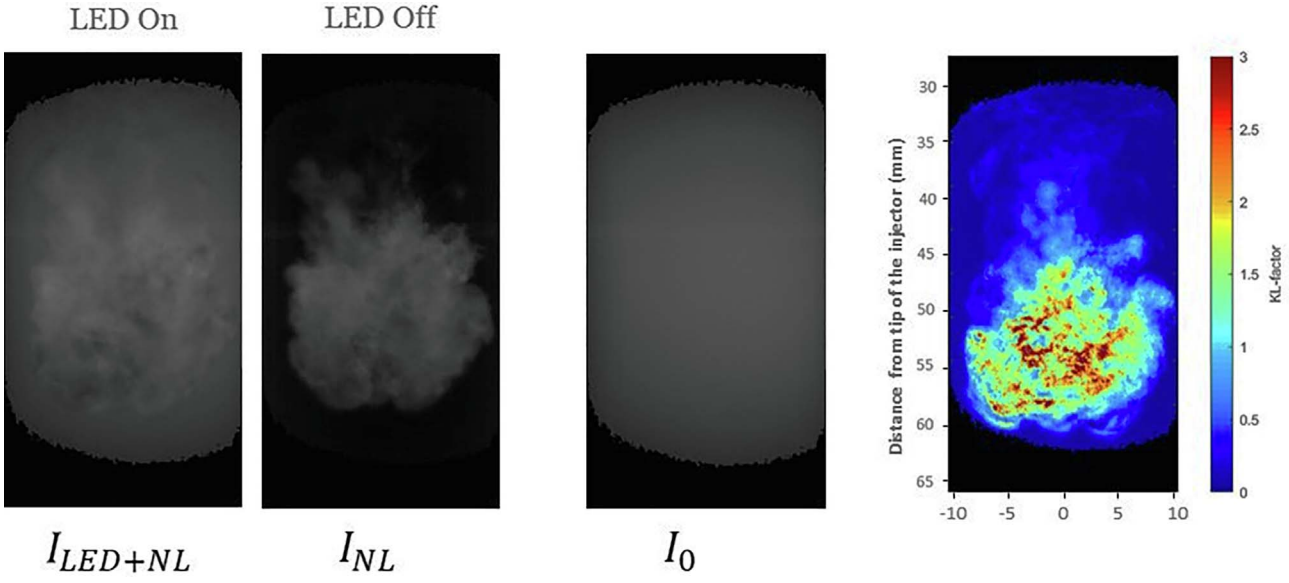

Fig. 3. Steps for the post processing of the KL factor.

The image presented in the right-most panel of Figure 3 corresponds to the processed image: a 2D distribution of soot extinction, KL.

The soot mass can be estimated by equation (5), with ρ_{soot}, the soot density, considered as 1.8 g/cm^3 as in [24], k_e, the non-dimensional extinction coefficient, set at 7.46 as in [25] and dx, dy the pixel sizes, here 11.2 µm/pix,

$$m_{soot} = \frac{\lambda_{LED}\,\rho_{soot}}{k_e}\,\mathrm{d}x \int_{-R}^{R} \mathrm{KL}\,\mathrm{d}y. \qquad (5)$$

3 Results

This section is divided into three parts. The first part focuses on the comparison between the results obtained in the reference condition, *i.e.* 15% O_2, 85% N_2 and the ECN pre-burn condition, namely with CO_2 and H_2O residue from the pre-combustion (15% O_2, 75.15% N_2, 6.22% CO_2, and 3.63% H_2O). The second and the third parts will cover the effects of CO_2 and water vapour addition on the flame soot, respectively.

3.1 Effect of pre-burn products

Figure 4 presents an example of the soot extinction images obtained at 15% O_2, 75.15% N_2, 6.33% CO_2, and 3.62% H_2O, representing ECN pre-burn conditions in comparison with those obtained without any exhaust gases *i.e.* the reference condition of 15% O_2 and 85% N_2, the reference condition, from 1.022 ms to 1.689 ms after the start of injection. For the two cases, the soot area increases with the combustion development. Soot formation starts in the periphery of the jet, due to the higher temperature and comparatively leaner mixture in the surrounding as compared to the central part of the jet [26]. During the flame development, soot volume fraction increases at the core of the jet (images from 1.378 ms to 1.689 ms) and stabilizes at the periphery. According to Cenker *et al.* [26] the air entrainment increases, soot first starts to oxidize in oxygen-rich high-temperature

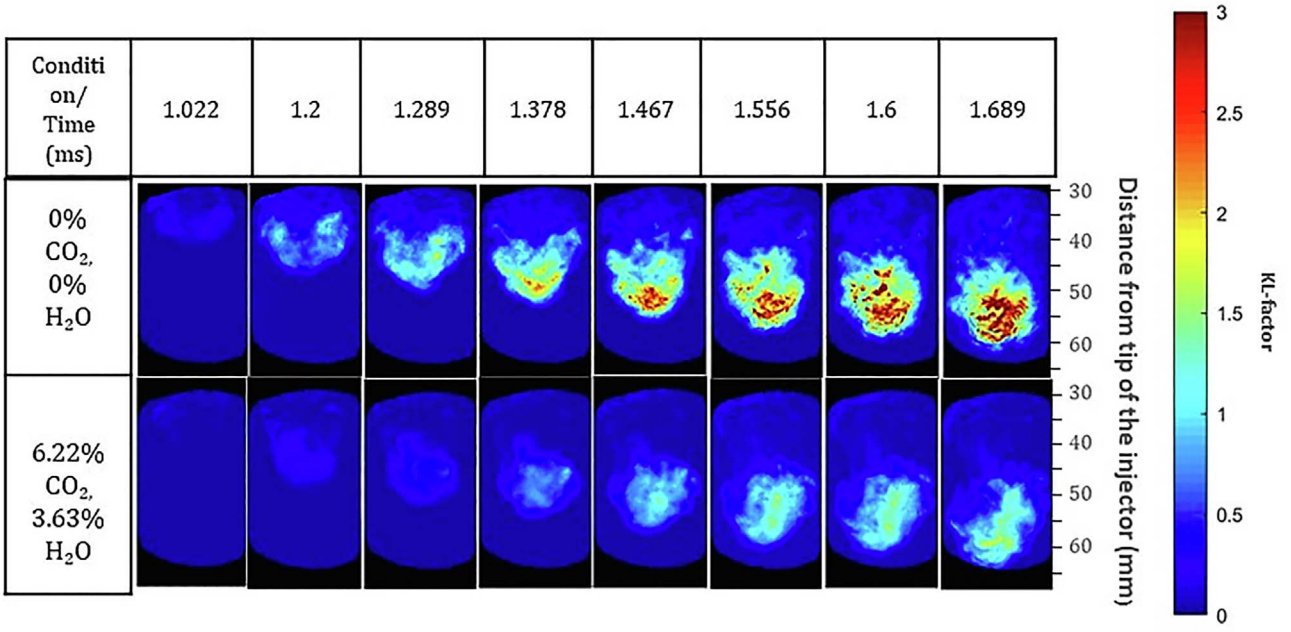

Fig. 4. Example of soot extinction images – comparison with ECN preburn gases composition and no exhaust gases in ambient gases (reference case).

zones such as the boundaries of the jet. The highest level of soot extinction is observed at the head of the front at 1.689 ms. After this event, the head of the soot cloud is outside the observation area but traces of the soot are observed till ~4 ms for the tail of the flame.

In this example, two trends can be observed: the soot onset time is shifted when pre-burn gases are taken into account in the ambient gases, and the extinction level is decreased by at least half. Ten repetitive tests were conducted to determine an average image. The maximum soot extinction value is 3 for the ECN pre-burn condition, against 4.5 for the reference condition. In Figure 5, the average KL factor, normalized by the maximum value obtained for the reference case is plotted as a function of the time After the Start of Injection (ASOI).The temporal evolution of KL values follows the same pattern as that presented by Musculus and Pickett [27] or [11, 23]. KL values reach the maximum when the head of the jet passes through the field of view. Once the head of the jet has passed through this position, the tail of the flame appears in the observation window till ~4 ms. In this part, the KL factor decreases by 40% in the two cases.

Figure 6a presents the estimate of soot mass 50 mm from the injector tip for ECN and reference conditions. The soot mass is reduced by 50% with the presence of 6.22% CO_2 and 3.63% H_2O in the ambient gases. Figure 6b presents the comparison between the total soot mass for both conditions with the results obtained in [7], named "SNL CVP vessel". The soot mass fraction for the ECN condition with pre-burn constituents in the ambient gases is around half of 51 µg, obtained in reference conditions. The value of, 25 µg is in good agreement with the results obtained in the actual pre-burn vessel [9]. Thanks to this comparison, it is highlighted that this reduction can be mainly attributed to the presence of inert gases, here

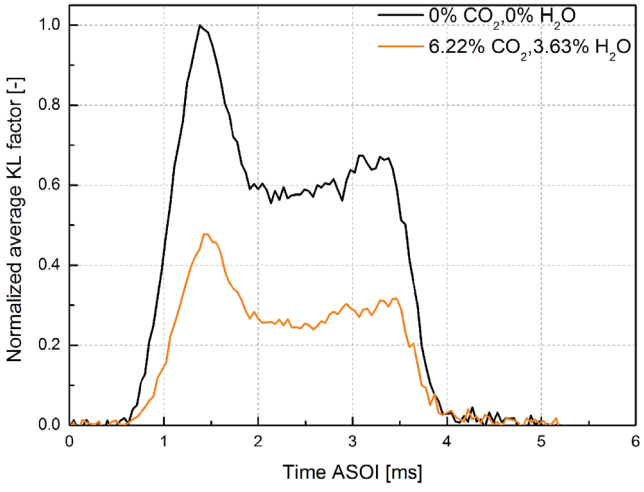

Fig. 5. Normalized average KL factor for ECN condition with pre-burn ambient gases composition and for reference condition, 15% O_2 and 85% N_2.

a mixture of CO_2 and H_2O, certainly due to the chemical reaction supported with dilution and thermal effects as discussed below.

3.2 Effects of CO_2 addition on soot

The average KL factor, obtained for 10 individual tests, and normalized by the maximum value obtained for the reference condition is presented in Figure 7a for the four amounts of CO_2. It can be clearly seen that the soot onset time is shifted. This shows that 2% CO_2 does not affect the soot extinction levels but that a significant decrease is obtained when at least 4.5% is added. In Figure 7b, the

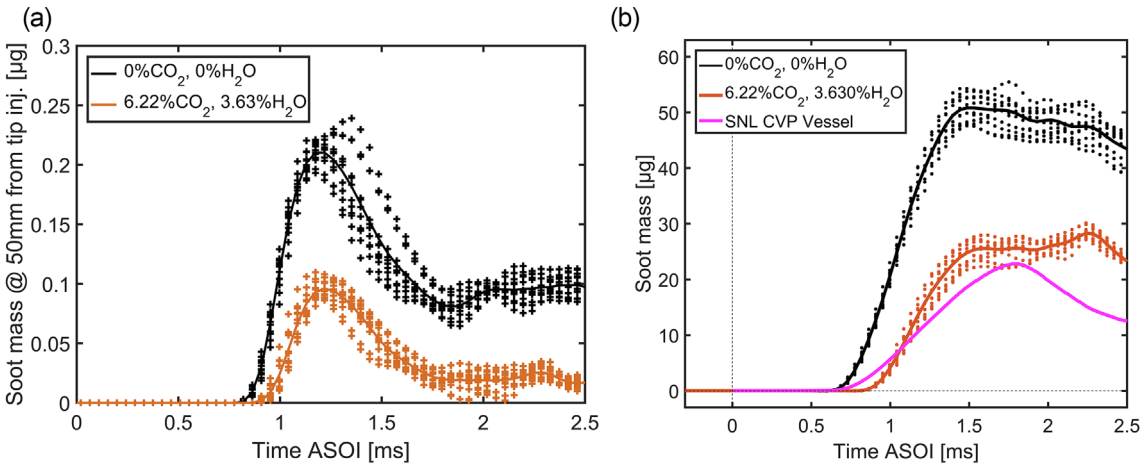

Fig. 6. (a) Soot mass 50 mm from the injector tip, (b) soot mass comparison with results in pre-burn vessel [9].

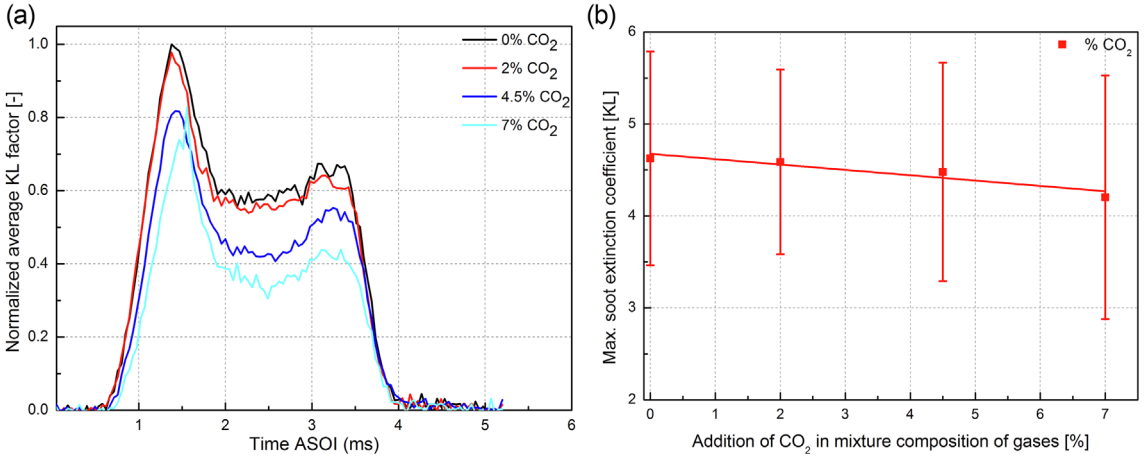

Fig. 7. (a) Normalized average KL factor *versus* time, (b) maximum of KL factor *versus* CO_2 content.

linear decrease of the maximum KL value is presented as a function of CO_2 content. For example, with 4.5% of CO_2 the maximum KL factor is decreased by 5.4%. These trends are also highlighted by the plot of the total soot mass estimate on the field of view (Fig. 8a). The highest quantity of total soot mass is observed for 0 and 2% CO_2 addition with a maximum at ~51 µg and ~48 µg respectively, while 4.5 and 7% addition of CO_2 decrease this maximum to ~43 µg and ~35 µg. Thus, a simple linear relationship can be suggested as expressed in equation (6) and seen in Figure 8b with a *R*-square of 0.97:

$$\frac{m_{\text{soot},\,\text{CO}_2\%}}{m_{\text{soot},\,0\%}} = 1 - 0.045 \cdot \text{CO}_2\%. \tag{6}$$

3.3 Effect of H_2O addition

The same trends can be observed with a variation in H_2O content from 1% to 5%: a shift of soot onset time and a reduction in the extinction level. However, as soon as 1% H_2O is introduced, a significant effect is observed on the average KL factor, with ~15% of reduction, as can be seen in Figure 9a. This trend is highlighted by the evolution of the maximum KL factor *versus* the percentage of H_2O, plotted in Figure 9b. A 20% reduction in this maximum is obtained when 5% H_2O is added.

Figure 10 presents the total soot mass (a) and the maximum soot mass reached between 1 ms and 2 ms after the start of injection (b) as a function of water vapour content in the ambient mixture. The impact on the soot mass is pronounced, as, the maximum value of total soot mass is reduced to 38% with 5% H_2O compared to the reference case. The following linear relationship (*R*-square = 0.95) can be suggested

$$\frac{m_{\text{soot},\,\text{H}_2\text{O}\%}}{m_{\text{soot},\,0\%}} = 1 - 0.066 \cdot \text{H}_2\text{O}\%. \tag{7}$$

4 Discussion

It was clearly observed that H_2O has a stronger effect on soot reduction than CO_2. For example, 2% of CO_2 or

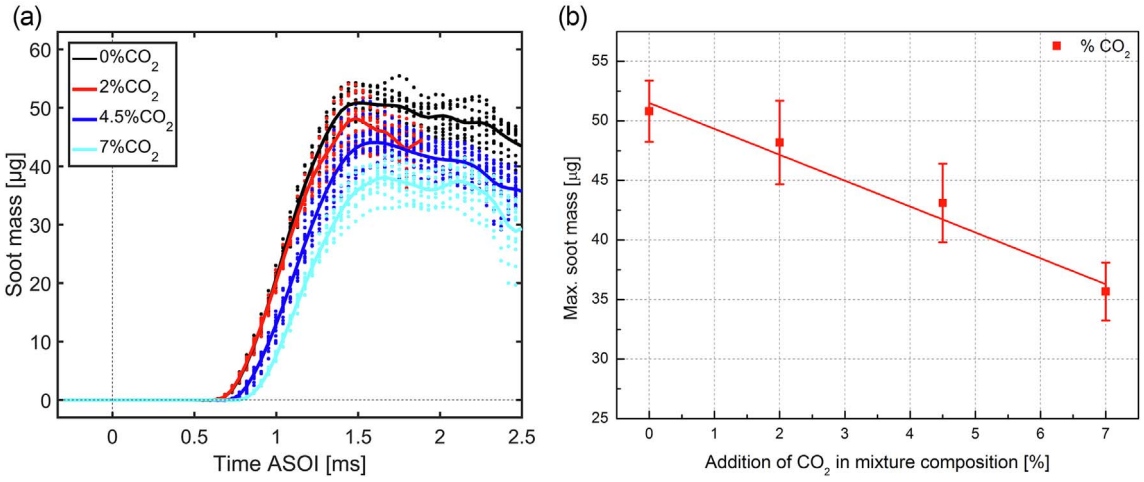

Fig. 8. Comparison of soot mass for different CO_2 content in ambient mixture (a) total soot mass, (b) maximum of soot mass between 1 ms and 2 ms ASOI.

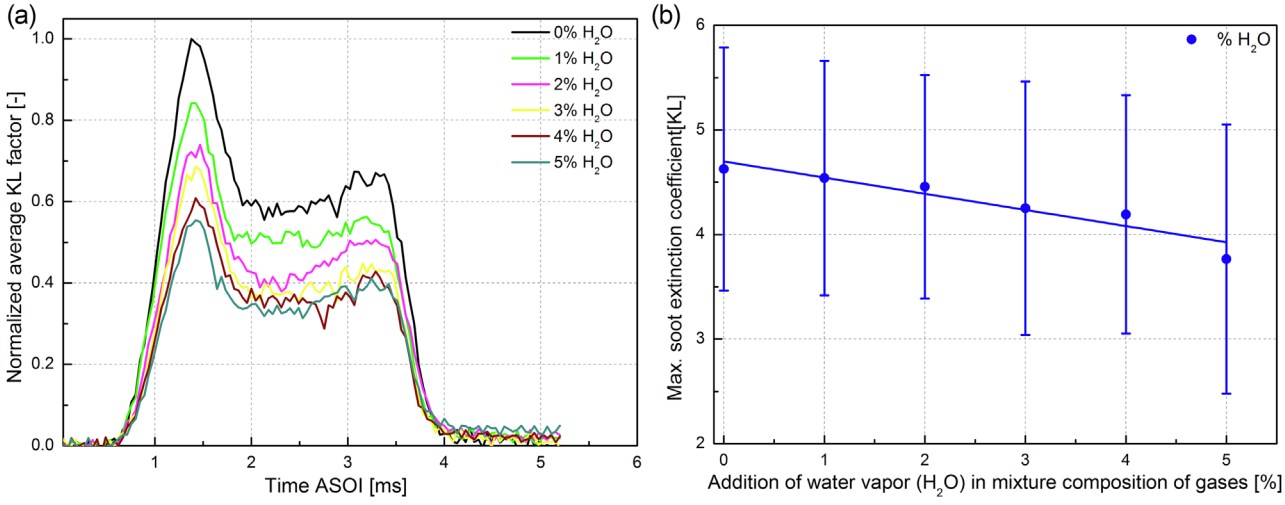

Fig. 9. (a) Normalized average KL factor as a function of H_2O content, (b) maximum soot extinction coefficient as a function of H_2O content.

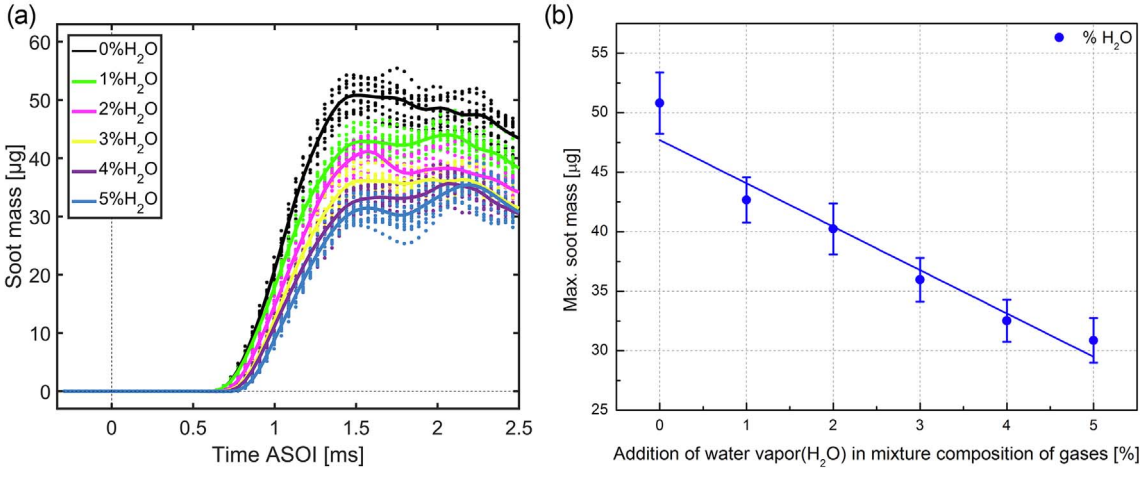

Fig. 10. Comparison of soot mass fraction as a function of H_2O content in mixture composition (a) total soot mass, (b) maximum soot mass between 1 ms and 2 ms ASOI.

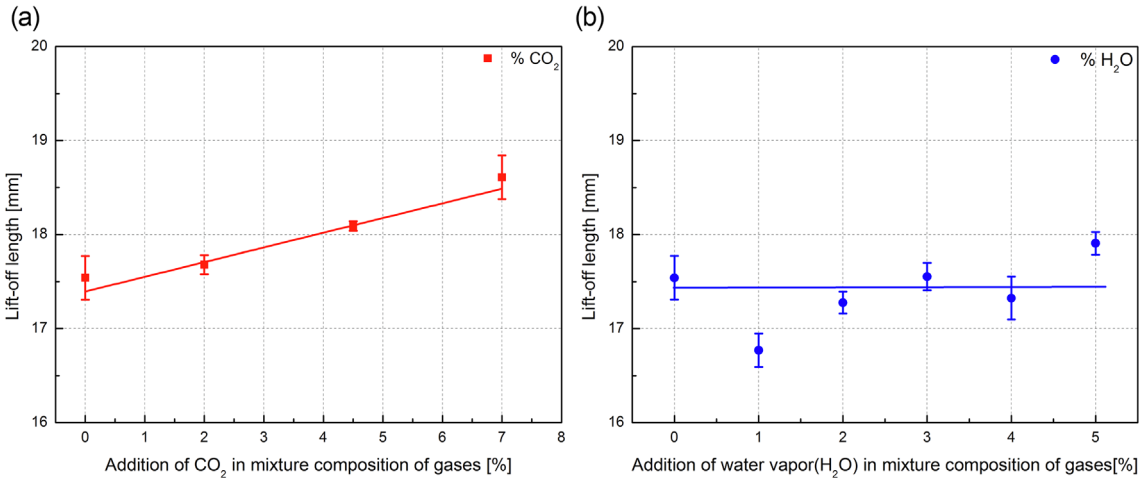

Fig. 11. Lift-off length as a function of the (a) CO_2 or (b) H_2O addition in ambient gases.

of H_2O resulted in a 5% and 20% reduction in the maximum soot value, respectively. Similar results were observed by Zhang *et al.* [6]. They found a more significant reduction of Polycyclic Aromatic Hydrocarbons (PAH) formation by H_2O when compared to CO_2 for the same blending ratio in laminar premixed $C_2H_4/O_2/Ar$ flames. The soot onset time is also more delayed with H_2O compared to CO_2.

The reduction in soot with the addition of CO_2 or H_2O in ambient gases can be attributed to different effects. First, due to the thermal capacities of these species in comparison to N_2, the flame temperature has to be reduced [28]. It can be noted that 7% CO_2 induced only a ~1.15% reduction in the adiabatic flame temperature (so from 957 K to 946 K) and 5% H_2O induced only a ~0.73% reduction in the adiabatic flame temperature (from 957 K to 950 K). As the impact on temperature is very small, other effects have to be considered according to [4].

The presence of CO_2 or H_2O in the ambient gases can also affect the location of the flame stabilization. This is highlighted in Figure 11 where an increase in the lift-off length can be noticed in the case of CO_2 (Fig. 11a) but not in the case of H_2O (Fig. 11b) as the variation is on the same order of variability. In fact the LOL depends on the initial ambient temperature [29] and in Table 2, the addition of CO_2 induces an initial temperature reduction of 11 K while only 6 K with the addition of H_2O. Figure 12 highlights the good correlation between LOL and the scaling law LOL* [29]. The variation in initial ambient temperature could explain the evolution of the LOL with addition of CO_2.

The flame with addition of CO_2 is stabilized in a leaner area, which could contribute to a soot reduction [29, 30]. However, as the effect of H_2O is greater than of CO_2, the soot reduction has to be mainly attributed according to [3, 5, 6, 31], to the chemical reactions.

In the case of CO_2, an interaction with H radicals such as $CO_2 + H \leftrightarrow OH + CO$, increases the amount of hydroxyl radicals, which enhances the oxidation process of the soot precursors. In the case of H_2O, as specified in [5], both

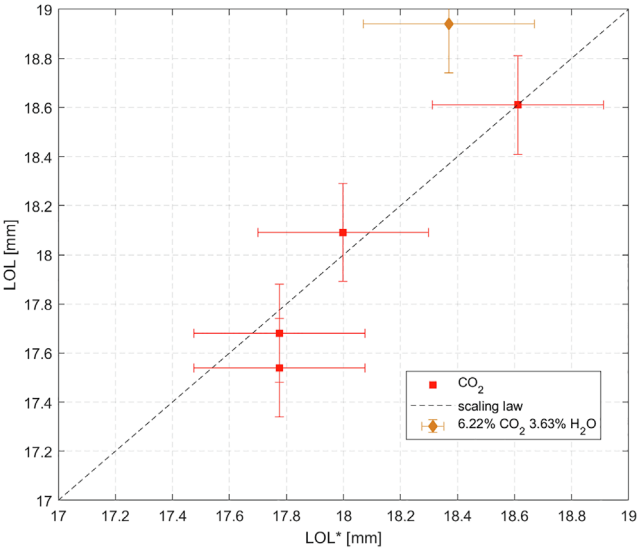

Fig. 12. LOL *versus* LOL* with addition of CO_2 $LOL^* = LOL_{ref}\left(\frac{T_{amb}}{T_{ref}}\right)^{-3,74}$ with $LOL_{ref} = 17,85$ mm and T_{ref}=900 K.

the reverse reactions of $H_2O + H \leftrightarrow OH + H_2$ and $H_2O + O \leftrightarrow OH + OH$ mainly contribute to reducing the formation of soot. According to Teini *et al.* [3], the addition of CO_2 and H_2O influences the growth of OH radicals in different areas of the flame. While CO_2 may begin to deplete soot mass through OH radical attacks in the oxidation zone, H_2O, inhibited PAH molecule growth reactions in fuel rich, soot formation regions. It results in the higher reduction of soot with H_2O addition as compared to CO_2.

5 Conclusion

Thanks to the NOSE experimental set-up, the effects of presence of CO_2 and H_2O in ambient mixtures on soot

formation were evaluated for the first time in the case of dodecane spray combustion. It was clearly observed that H_2O has a stronger effect on soot reduction than CO_2, as previously observed in ethane flames. The soot reduction is certainly due to reactions between H radicals and CO_2 or H_2O and between O radical and H_2O. The reactions promote OH radicals which are reduced by oxidation in PAH. By combining CO_2 and H_2O in the ambient mixture as in real ECN pre-burn conditions, a reduction of 50% in comparison to the reference condition ($15\%O_2 + 85\%N_2$) is estimated and is in very good agreement by real measurements in a pre-burn vessel. This confirms that the presence of these species has to be considered in any simulations of results for ECN pre-burn vessels in order to increase the model prediction accuracy.

Acknowledgments. The authors acknowledge the National Research Agency (contract ANR-14-CE22-0015-01) for financial support to the ECN-France project and Region Centre Val de Loire (CPER 2007-2013 Energies du Futur) and FEDER for financial support to build the NOSE set-up. The authors thank H. Ajrouche, O. Nilaphai, Y. Haidous, and B. Moreau for helping with the experiments. The authors greatly acknowledge the valuable discussions with G. Bruneaux.

References

1 Durant J.L., Busby W.F., Lafleur A.L., Penman B.W., Crespi C.L. (1996) Human cell mutagenicity of oxygenated, nitrated and unsubstituted polycyclic aromatic hydrocarbons associated with urban aerosols, *Mutat. Res. Toxicol.* **371**, 123–157. doi: 10.1016/S0165-1218(96)90103-2.

2 Kumfer B.M., Skeen S.A., Axelbaum R.L. (2008) Soot inception limits in laminar diffusion flames with application to oxy–fuel combustion, *Combust. Flame* **154**, 546–556. doi: 10.1016/J.COMBUSTFLAME.2008.03.008.

3 Teini P.D., Karwat D.M.A., Atreya A. (2012) The effect of CO_2/H_2O on the formation of soot particles in the homogeneous environment of a rapid compression facility, *Combust. Flame* **159**, 1090–1099. doi: 10.1016/j.combustflame.2011.10.002.

4 Du D.X., Axelbaum R.L., Law C.K. (1991) The influence of carbon dioxide and oxygen as additives on soot formation in diffusion flames, *Symp. Combust.* **23**, 1501–1507. doi: 10.1016/S0082-0784(06)80419-4.

5 Liu F., Consalvi J.L., Fuentes A. (2014) Effects of water vapor addition to the air stream on soot formation and flame properties in a laminar coflow ethylene/air diffusion flame, *Combust. Flame* **161**, 1724–1734. doi: 10.1016/j.combustflame.2013.12.017.

6 Zhang Y., Wang L., Liu P., Guan B., Ni H., Huang Z., Lin H. (2018) Experimental and kinetic study of the effects of CO_2 and H_2O addition on PAH formation in laminar premixed $C_2H_4/O_2/Ar$ flames, *Combust. Flame* **192**, 439–452. doi: 10.1016/j.combustflame.2018.01.050.

7 Hoerlle C.A., Pereira F.M. (2019) Effects of CO_2 addition on soot formation of ethylene non-premixed flames under oxygen enriched atmospheres, *Combust. Flame* **203**, 407–423. doi: 10.1016/j.combustflame.2019.02.016.

8 Ying Y., Liu D. (2019) Effects of water addition on soot properties in ethylene inverse diffusion flames, *Fuel* **247**, 187–197. doi: 10.1016/j.fuel.2019.03.034.

9 Engine Combustion Network (2019) [online] Available from https://ecn.sandia.gov.

10 Skeen S.A., Manin J., Pickett L.M., Cenker E., Bruneaux G., Kondo K., Aizawa T., Westlye F., Dalen K., Ivarsson A., Xuan T.A. (2016) Progress review on soot experiments and modeling in the Engine Combustion Network (ECN), *SAE Int. J. Engines* **9**, 883–898. doi: 10.4271/2016-01-0734.

11 Skeen S., Yasutomi K., Cenker E., Adamson B., Hansen N., Pickett L. (2018) Standardized optical constants for soot quantification in high-pressure sprays, *SAE Int. J. Engines* **11**, 805–816. doi: 10.4271/2018-01-0233.

12 Westlye F.R., Penney K., Ivarsson A., Pickett L.M., Manin J., Skeen S.A. (2017) Diffuse back-illumination setup for high temporally resolved extinction imaging, *Appl. Opt.* **56**, 5028–5038. doi: 10.1364/ao.56.005028.

13 Ghandhi J.B., Heim D.M. (2009) An optimized optical system for backlit imaging, *Rev. Sci. Instrum.* **80**, 056105. doi: 10.1063/1.3128728.

14 Manin J., Bardi M., Pickett L.M., Dahms R.N., Oefelein J.C. (2014) Microscopic investigation of the atomization and mixing processes of diesel sprays injected into high pressure and temperature environments, *Fuel* **134**, 531–543. doi: 10.1016/j.fuel.2014.05.060.

15 Xue Q., Som S., Senecal P.K., Pomraning E. (2013) Large eddy simulation of fuel-spray under non-reacting ic engine conditions, *At. Sprays* **23**, 925–955. doi: 10.1615/atomizspr.2013008320.

16 Luo Z., Som S., Sarathy S.M., Plomer M., Pitz W.J., Longman D.E., Lu T. (2014) Development and validation of an n-dodecane skeletal mechanism for spray combustion applications, *Combust Theory Model* **18**, 187–203. doi: 10.1080/13647830.2013.872807.

17 Hiroyasu H., Kadota T. (1976) Models for combustion and formation of nitric oxide and soot in direct injection diesel engines, *SAE Tech. Pap. Ser.*, 760129. doi: 10.4271/760129.

18 Wang H., Ra Y., Jia M., Reitz R.D. (2014) Development of a reduced n-dodecane-PAH mechanism and its application for n-dodecane soot predictions, *Fuel* **136**, 25–36. doi: 10.1016/j.fuel.2014.07.028.

19 Vishwanathan G., Reitz R.D. (2010) Development of a practical soot modeling approach and its application to low-temperature diesel combustion, *Combust. Sci. Technol.* **182**, 1050–1082. doi: 10.1080/00102200903548124.

20 Ajrouche H., Nilaphai O., Hespel C., Foucher F. (2019) Impact of nitric oxide on n-heptane and n-dodecane autoignition in a new high-pressure and high-temperature chamber, *Proc. Combust. Inst.* **37** 3319–3326. doi: 10.1016/j.proci.2018.07.102.

21 Ben Houidi M., Hespel C., Bardi M., Nilaphai O., Malbec L.-M., Sotton J., Bellenoue M., Strozzi C., Ajrouche H., Foucher F., Moreau B., Rousselle C., Bruneaux G. (2019) Characterization of the ECN spray A in different facilities. Part 1: boundary conditions characterization. *Oil Gas Sci. Technol. - Rev. IFP Energies nouvelles*. doi: 10.2516/ogst/2020023.

22 Payri R., Salvador F.J., Manin J., Viera A. (2016) Diesel ignition delay and lift-off length through different methodologies using a multi-hole injector, *Appl. Energy* **162**, 541–550. doi: 10.1016/j.apenergy.2015.10.118.

23 Lind T., Roberts G., Eagle W., Rousselle C., Andersson Ö., Musculus M.P. (2018) Mechanisms of post-injection soot-reduction revealed by visible and diffused back-illumination soot extinction imaging, *SAE Tech. Pap. Ser.* doi: 10.4271/2018-01-0232.

24 Manin J., Skeen S., Pickett L., Kurtz E., Anderson J.E. (2014) Effects of oxygenated fuels on combustion and soot formation/oxidation processes, *SAE Int. J. Fuels Lubr.* **7**, 704–717. doi: 10.4271/2014-01-2657.

25 Manin J., Pickett L.M., Skeen S.A. (2013) Two-color diffused back-illumination imaging as a diagnostic for time-resolved soot measurements in reacting sprays, *SAE Int. J. Engines* **6**, 1908–1921. doi: 10.4271/2013-01-2548.

26 Cenker E., Bruneaux G., Pickett L., Schulz C. (2013) Study of soot formation and oxidation in the Engine Combustion Network (ECN), spray A: Effects of ambient temperature and oxygen concentration, *SAE Int. J. Engines* **6**, 352–365. doi: 10.4271/2013-01-0901.

27 Musculus M.P.B., Pickett L.M. (2005) Diagnostic considerations for optical laser-extinction measurements of soot in high-pressure transient combustion environments, *Combust. Flame* **141**, 371–391. doi: 10.1016/j.combustflame.2005.01.013.

28 Liu F., Guo H., Smallwood G.J., Gülder Ö.L. (2001) The chemical effects of carbon dioxide as an additive in an ethylene diffusion flame: Implications for soot and NOx formation, *Combust. Flame* **125**, 778–787. doi: 10.1016/S0010-2180(00)00241-8.

29 Donkerbroek A.J., Boot M.D., Luijten C.C.M., Dam N.J., ter Meulen J.J. (2011) Flame lift-off length and soot production of oxygenated fuels in relation with ignition delay in a DI heavy-duty diesel engine, *Combust. Flame* **158**, 525–538. doi: 10.1016/j.combustflame.2010.10.003.

30 Pickett L.M., Siebers D.L. (2004) Soot in diesel fuel jets: Effects of ambient temperature, ambient density, and injection pressure, *Combust Flame* **138**, 114–135. doi: 10.1016/J.COMBUSTFLAME.2004.04.006.

31 Lentati A.M., Chelliah H.K. (1998) Dynamics of water droplets in a counterflow field and their effect on flame extinction, *Combust. Flame* **115**, 158–179. doi: 10.1016/S0010-2180(97)00355-6.